# Fine-Tuning Nickel Phenoxyimine Olefin Polymerization Catalysts: Performance Boosting by Alkali Cations

Zhongzheng Cai, Dawei Xiao, and Loi H. Do*

Department of Chemistry, University of Houston, 4800 Calhoun Road, Houston, Texas 77004, United States

Ⓢ Supporting Information

ABSTRACT: To gain a better understanding of the influence of cationic additives on coordination−insertion polymerization and to leverage this knowledge in the construction of enhanced olefin polymerization catalysts, we have synthesized a new family of nickel phenoxyimine−polyethylene glycol complexes (**NiL0, NiL2−NiL4**) that form discrete molecular species with alkali metal ions (M$^+$ = Li$^+$, Na$^+$, K$^+$). Metal binding titration studies and structural characterization by X-ray crystallography provide evidence for the self-assembly of both 1:1 and 2:1 **NiL**:M$^+$ species in solution, except for **NiL4**/Na$^+$ which form only the 1:1 complex. It was found that upon treatment with a phosphine scavenger, these **NiL** complexes are active catalysts for ethylene polymerization. We demonstrate that the addition of M$^+$ to **NiL** can result in up to a 20-fold increase in catalytic efficiency as well as enhancement in polymer molecular weight and branching frequency compared to the use of **NiL** without coadditives. To the best of our knowledge, this work provides the first systematic study of the effect of secondary metal ions on metal-catalyzed polymerization processes and offers a new general design strategy for developing the next generation of high performance olefin polymerization catalysts.
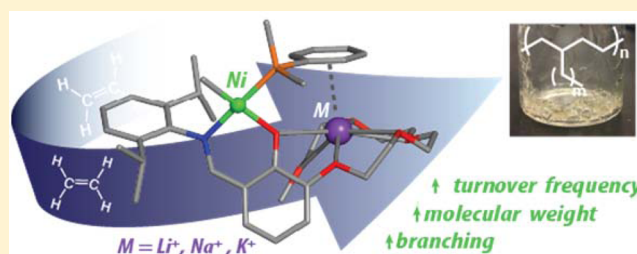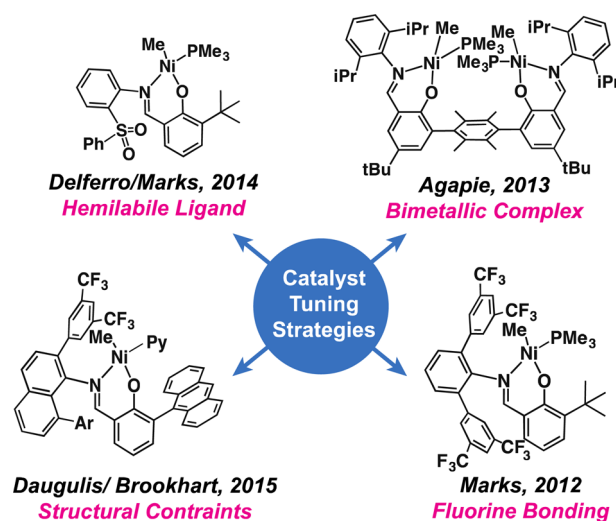
INTRODUCTION

The discovery that homogeneous late transition metal catalysts can exhibit olefin polymerization activity similar to that of early transition metal catalysts led to a major paradigm shift in olefin polymerization catalysis.[1−12] Because late transition metal catalysts (e.g., Ni, Pd) are far less susceptible to inhibition by heteroatom donors compared to their early transition metal counterparts (e.g., Ti, Hf, Zr), the former typically exhibit greater tolerance of polar monomers, solvents, and impurities compared to the latter. Although recent developments in nickel and palladium catalysis have led to the creation of systems that can copolymerize ethylene and polar vinyl monomers through a coordination−insertion mechanism,[13−15] the resulting polymers tend to have low molecular weight and the catalyst activity tends to be poor. To have utility in commercial polymer synthesis,[9] the ideal catalyst should have high catalytic efficiency, be thermally robust, yield polymers with high molecular weight and narrow polydispersity, and display good control over polymer microstructure.

In an effort to engineer catalysts that satisfy the stringent requirements above, a variety of design strategies have been explored. Some of the most notable examples are shown in Chart 1, which include the use of structural constraints,[16−21] fluorine bonding,[22,23] hemilabile ligands,[24] and bimetallic active sites.[25−29] One of the key findings from these studies is that sterically bulky ligands that protect the axial sites of square planar nickel and palladium complexes tend to promote polymer chain elongation over chain transfer, which can lead to the formation of ultrahigh molecular weight polymers (e.g.,

Chart 1. Examples of Design Strategies Explored in the Development of Improved Nickel Phenoxyimine Olefin Polymerization Catalysts

Delferro/Marks, 2014
Hemilabile Ligand

Agapie, 2013
Bimetallic Complex

Catalyst Tuning Strategies

Daugulis/ Brookhart, 2015
Structural Contraints

Marks, 2012
Fluorine Bonding

M_n up to 3×10^6 g/mol)[20] and give catalysts that show "quasi-living" behavior.[30] It has also been suggested that weak C(ligand)−F⋯H−C(polymer) interactions through fluorine

bonding of a catalyst with a growing polymer chain can help suppress β-hydride elimination to furnish linear polyethylene.[22]

In our goal to develop high performance catalysts for the controlled polymerization of olefins, our laboratory is interested in the application of dual metal catalysis.[31] There is compelling evidence that bimetallic complexes, such as those based on the double-decker[27,28] or arene-bridged structures,[25,26] allow for better incorporation of polar comonomers compared to mononuclear catalysts due to the presence of metal–metal cooperativity.[12,32] Most of the bimetallic catalysts reported in the literature, however, contain metal centers that are both active in olefin polymerization (or trimerization/oligomerization in some cases). In our research, we wish to explore the olefin polymerization behavior of complexes that comprise two functionally distinct metal centers,[33–35] where one metal ion carries out olefin polymerization and the other serves as an activator and binding site for polar functionalities. We hypothesize that such site-differentiated heterobimetallic species can enhance the coordination–insertion of olefins compared to homobimetallic species because the two metal centers do not compete with each other for monomer binding and there is no steric interference from two growing polymer chains within the same catalyst structure.

As proof of concept, we have prepared a new class of nickel complexes supported by phenoxyimine ligands having pendant polyethylene glycol (PEG) side chains.[36–38] We show that the spontaneous self-assembly of dinuclear nickel–alkali metal complexes generates highly active catalysts for ethylene polymerization, which displays a remarkable increase in polymer branching, molecular weight, and turnover frequency compared to polymerizations performed in the absence of alkali metal ions. These findings demonstrate the beneficial effects of cationic Lewis acids on olefin polymerization and provide a new conceptual framework with which to guide future catalyst design efforts.

■ RESULTS AND DISCUSSION

Catalyst Design Rationale and Synthesis. We were inspired by a literature report demonstrating that nickel phosphine–alkoxide complexes were more productive in the copolymerization of ethylene and hexyl acrylate when excess $LiB(C_6F_5)_4$ salts were used as coadditives.[39] Although the authors reported that the precatalysts used in the study have dinuclear nickel–lithium structures, the precise role of the lithium cations in polymerization was not further elaborated. In our work, we were intrigued by the possibility that "hard" Lewis acids such as group I and II metal ions might exhibit metal–metal cooperativity in olefin polymerization when paired with a conventional nickel catalyst. We postulate that having two functionally distinct metal centers within a single catalyst scaffold would impart new reactivity patterns that are not accessible using homobimetallic catalysts. Furthermore, we favor using alkali and alkaline cations as the secondary metal because they do not engage in redox reactions and form relatively stable metal–ligand interactions with hard Lewis bases such as the carbonyl groups of polar monomers (e.g., acrylate, acrylamide, etc.).

To obtain discrete heterobimetallic complexes, we prepared a new family of dinucleating ligands based on the phenoxyimine platform (Scheme 1).[14] Polyethylene glycol (PEG) moieties containing 0–4 ethylene glycol units were attached to the phenol ring of N-(2,6-diisopropylphenyl)phenoxyimine to yield a series of ligands **HL** (the ligand number specifies the number

Scheme 1. Synthesis of NiL0, NiL2–NiL4[a]
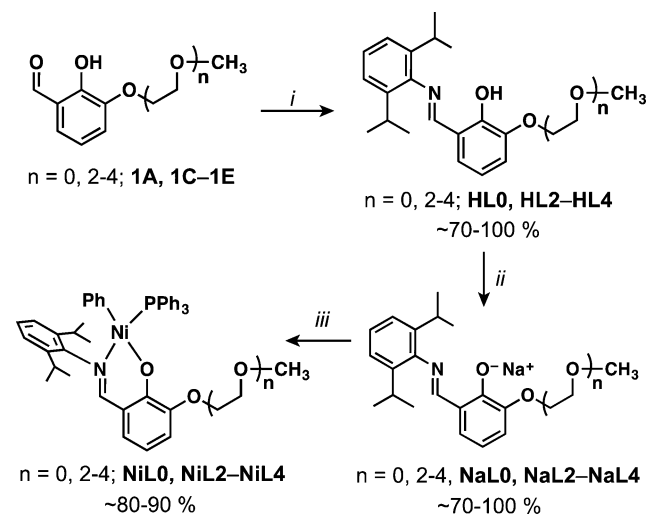
[a]Reaction conditions: (i) 2,6-diisopropylaniline, acetic acid, MeOH; (ii) sodium hydride, THF; (iii) NiBr(Ph)(PPh$_3$)$_2$, THF. The phenoxyimine ligands are denoted as **L**, followed by a number to indicate the length of the PEG chain attached to the phenol unit of the ligand.

of ethylene glycol units in the PEG chain). The *O*,*N*-chelate of the phenoxyimine unit will be ligated to nickel, whereas the PEG/phenolate groups will be ligated to either a group I or II cation. Having different **HL** variants will allow us to determine the optimal PEG chain length required to accommodate cations with different ionic radii.[37,38,40] The **HL** ligands are modular and simple to prepare starting from commercially available precursors.

The **HL** ligands were synthesized according to the procedure depicted in Scheme 1. The aldehydes **1A/1C–1E** were obtained from alkylation of 2,3-dihydroxybenzaldehye by treatment with sodium hydride, followed by reaction with the appropriate tosyl-PEG or bromo-PEG reagent.[36] Reaction of the 3-alkylated compound **1** with 2,6-diisopropylaniline and acetic acid afforded ligands **HL** in moderate to excellent yields (70–100%).
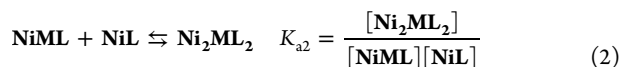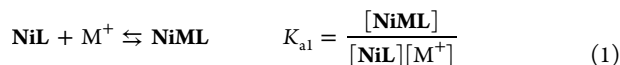
Metalation of **HL** was accomplished by first treatment of the ligands with sodium hydride, which yielded **NaL** as yellow solids (Scheme 1). The phenolate salt was then combined with the nickel precursor Ni(Br)(Ph)(PPh$_3$)$_2$ to give the Ni(Ph)-(PPh$_3$)(L) complexes **NiL** in good yields (80–90%). X-ray crystallographic characterization of Ni(Mes)(PPh$_3$)(L2) (**NiL2$_{Mes}$**, where Mes = 2,4,6-trimethylphenyl), which was prepared from the reaction of Ni(Br)(Mes)(PPh$_3$)$_2$ with **NaL2**, shows that the nickel center adopts a square planar geometry, in which the aryl group is coordinated *trans* to the phenolate donor (Figure 1).

Metal Binding Studies. With the **NiL** complexes in hand, we performed metal ion titration studies by UV–vis absorption spectroscopy to examine their metal binding behavior. For these experiments, solutions containing 100 μM **NiL** (i.e., **NiL2**, **NiL3**, or **NiL4**) in Et$_2$O were treated with aliquots of 0.1 equiv of MBAr$^F_4$ salts (M = Li$^+$, Na$^+$, and K$^+$; BAr$^F_4^-$ = tetrakis(3,5-trifluoromethylphenyl)borate) and then allowed to equilibrate for ~20–30 min before recording the spectral changes. Upon addition of the alkali metal salts, the absorption bands centered at ~340 and ~420 nm decreased, whereas the absorbance at ~375 nm increased (Figure 2 and Figure S1).
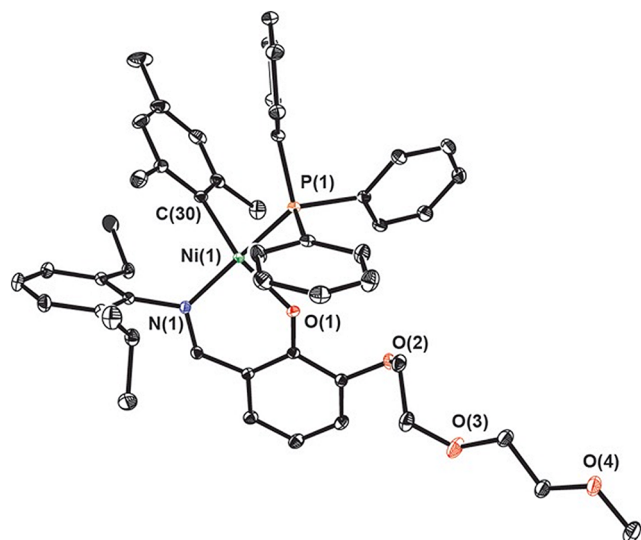
Figure 1. X-ray crystal structure of $Ni(Mes)(PPh_3)(L2)$ ($NiL2_{Mes}$, ORTEP view, displacement ellipsoids drawn at 50% probability level). Hydrogen atoms and solvent have been omitted for clarity.

Titration studies could not be performed with **NiL0** or using alkaline salts (e.g., $Mg(SO_3CF_3)_2$, $Ca(SO_3CF_3)_2$) due to their poor solubility in Et_2O. The titration plots show that the complexation of M^+ to **NiL** does not follow a simple A→ B binding model due to the lack of any clear isosbestic points, except for the reaction of Na^+ with **NiL4**. The introduction of $NaBAr^F_4$ to a solution of **NiL4** led to the development of clean isosbestic points at 360 and 405 nm (Figure 2B). The spectral data obtained from these titration studies were fit using nonlinear least-squares regression by the program DynaFit.[41] The following chemical equilibria were used in the data fitting:

$$NiL + M^+ \leftrightarrows NiML \qquad K_{a1} = \frac{[NiML]}{[NiL][M^+]} \qquad (1)$$

$$NiML + NiL \leftrightarrows Ni_2ML_2 \qquad K_{a2} = \frac{[Ni_2ML_2]}{[NiML][NiL]} \qquad (2)$$

where **NiML** is the 1:1 **NiL**:M^+ complex $[NiM(Ph)(PPh_3)-(L)]^+$, **Ni2ML2** is the 2:1 **NiL**:M^+ complex $[Ni_2M-(Ph)_2(PPh_3)_2(L)_2]^+$, and the K_a values are their corresponding association constants. In almost all cases, the absorbance changes at 340 nm fit better to a model involving the formation of both 1:1 and 2:1 species compared to one involving just the formation of the 1:1 species (Figure 2A inset and Figure S2). Only the titration data for **NiL4**/Na^+ fit well to a simple 1:1 binding model (Figure 2B inset). As shown in Table 1, K_{a1} values are in the range of $(0.23-26.66) \times 10^{-2} \mu M^{-1}$, whereas K_{a2} values are in the range of $(0.55-2.73) \times 10^{-2} \mu M^{-1}$. These data are consistent with the observed trend that the most stable alkali-PEG complexes are formed when the PEG chain length matches the ionic radius of the metal ion.[37,38,40] For example, the K_{a1} values for **NiL3** are 0.77-, 5.76-, and $4.50 \times 10^{-2} \mu M^{-1}$ with Li^+, Na^+, and K^+, respectively, which indicate that **NiL3** containing a triethylene glycol unit binds to Na^+ better than to either Li^+ or K^+. The most stable 1:1 complex is formed between **NiL4** and Na^+, with a K_{a1} value of $26.66 \times 10^{-2} \mu M^{-1}$, which is a significantly higher association constant compared to other **NiL** complexes with M^+. These metal binding studies suggest that the speciation of the **NiL** complexes can differ in solution due to the specific alkali ions used, which has
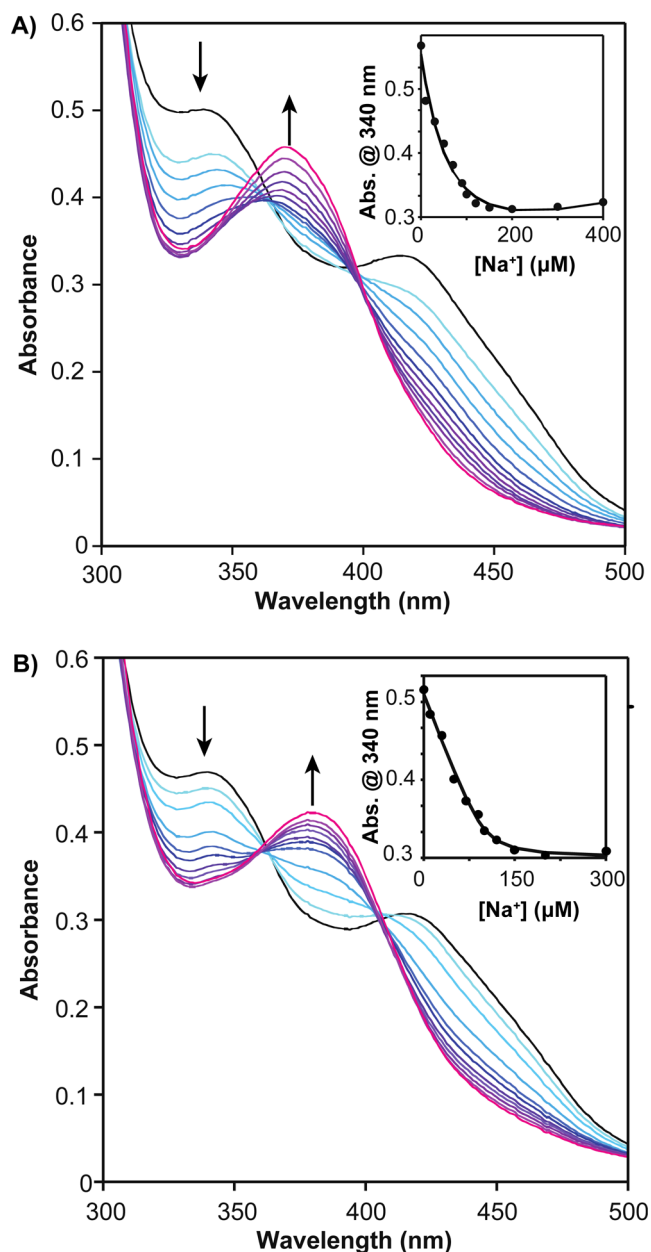
Figure 2. Metal titration plots showing the spectral changes due to the addition of $NaBAr^F_4$ to A) **NiL2** and B) **NiL4** in Et_2O (100 μM). The black traces are the starting spectra of **NiL** and the colored traces are the spectra obtained after the addition of 0.1 equiv of Na^+, relative to Ni. The insets show the absorbance changes at 340 nm as black dots and the DynaFit nonlinear regression fit as black solid lines.

Table 1. Association Constants K_{a1} and K_{a2} Determined from Metal Titration Studies[a]

complex	Li^+	Na^+	K^+
NiL2	1.09 (K_{a1})	0.23 (K_{a1})	0.75 (K_{a1})
	0.63 (K_{a2})	2.73 (K_{a2})	0.60 (K_{a2})
NiL3	0.77 (K_{a1})	5.74 (K_{a1})	4.50 (K_{a1})
	0.76 (K_{a2})	0.58 (K_{a2})	0.55 (K_{a2})
NiL4	1.65 (K_{a1})	26.66 (K_{a1})	1.83 (K_{a1})
	0.92 (K_{a2})	–	0.71 (K_{a2})

[a]The association constants have units of $\times 10^{-2} \mu M^{-1}$.

important implications in their olefin polymerization activity as described below.
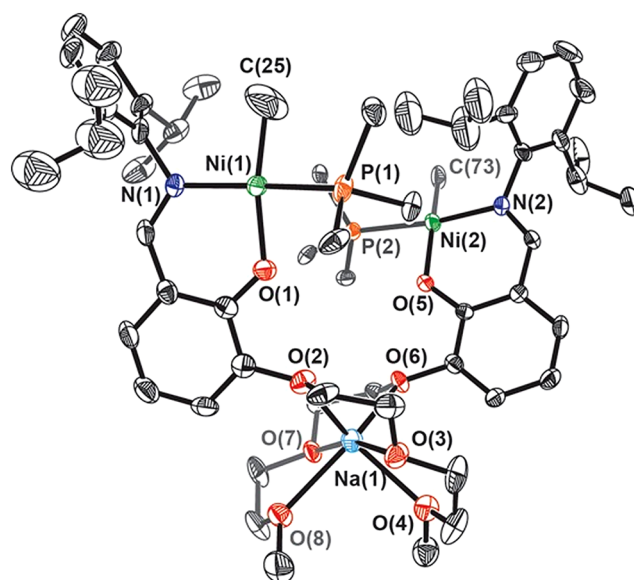
Structural Characterization. The metal binding studies above strongly suggest that both 1:1 **NiML** and 2:1 **Ni$_2$ML$_2$** complexes are formed in solution. To obtain evidence for such species and to determine their molecular structures, single crystals of the nickel-alkali complexes were prepared and analyzed by X-ray crystallography. To obtain crystals of [NiNa(Ph)(PPh$_3$)(L3)](BAr$^F_4$) (**NiNaL3**), **NiL3** and NaBAr$^F_4$ (1:1) were combined in Et$_2$O and then layered with pentane to give orange-colored blocks upon standing for several days. The X-ray structure of **NiNaL3** is shown in Figure 3A. As expected, the nickel center adopts a square planar geometry with the phenyl group coordinated *trans* to the phenolate donor. The sodium cation is ligated by the phenolate group (Na(1)−O(1) = 2.52 Å) and four oxygen donors from the PEG chain (Na(1)−O$_{ave}$ = ~2.43 Å)[42,43] and has a metal-π interaction with one of the phenyl rings of triphenylphosphine (Na(1)−

A)

B)
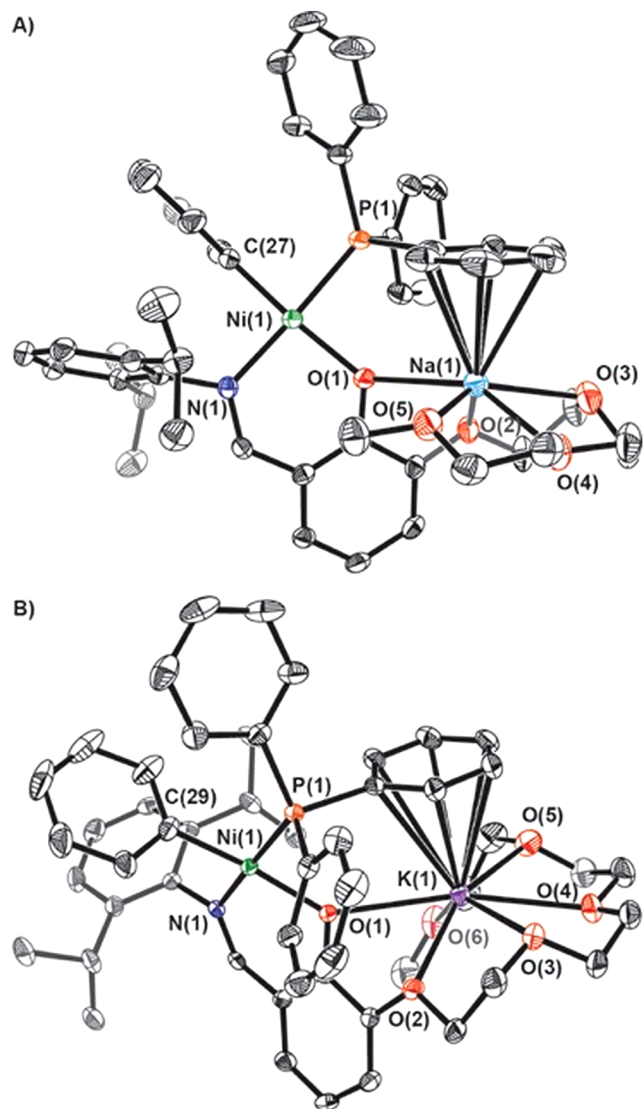
Figure 3. X-ray crystal structures of (A) [NiNa(Ph)(PPh$_3$)(L3)]-(BAr$^F_4$) (**NiNaL3**) and (B) [NiK(Ph)(PPh$_3$)(L4)](BAr$^F_4$) (**NiKL4**) shown in ORTEP view with displacement ellipsoids drawn at 50% probability level. Hydrogen atoms and the BAr$^F_4$$^-$ anions have been omitted for clarity.

Ph(centroid) = 2.64 Å).[44] Crystals of the [NiK(Ph)(PPh$_3$)-(L4)](BAr$^F_4$) complex (**NiKL4**) were grown by mixing **NiL4** and KBAr$^F_4$ (1:1) in Et$_2$O and layering with pentane. X-ray diffraction analysis reveals that the nickel center in **NiKL4** has a four-coordinate geometry (Figure 3B), similar to that in **NiNaL3**. The potassium ion is coordinated to the phenolate group (K(1)−O(1) = 2.84 Å) and six ether oxygen donors (K(1)−O$_{ave}$ = 2.79 Å)[45] as well as a phenyl ring from triphenylphosphine (K(1)−Ph(centroid) = 2.99 Å).[46]

To grow crystals of the 2:1 complex, **NiL2** and NaBAr$^F_4$ (2:1) were dissolved in benzene and the mixture was slowly diffused with pentane. The orange crystals obtained were analyzed by X-ray crystallography, which shows a compound with the molecular composition [Ni$_2$Na(Ph)$_2$(PPh$_3$)$_2$(L2)$_2$]-BAr$^F_4$ (**Ni$_2$NaL2$_2$**, Figure 4). Unlike the 1:1 **NiL**:M$^+$ structures,

Figure 4. X-ray crystal structure of [Ni$_2$Na(Ph)$_2$(PPh$_3$)$_2$(L2)$_2$](BAr$^F_4$) (**Ni$_2$NaL2$_2$**) shown in ORTEP view with displacement ellipsoids drawn at 50% probability level. The hydrogen atoms, BAr$^F_4$$^-$ anions, and phenyl rings have been omitted for clarity.

the alkali ion in **Ni$_2$NaL2$_2$** links two **NiL2** units together by binding to two separate diethylene glycol chains, resulting in a six-coordinate sodium center (Na(1)−O$_{ave}$ = 2.44 Å).[47]

A structural comparison between the mononuclear (**NiL2$_{Mes}$**) and dinuclear (**NiNaL3** and **NiKL4**) species shows some slight variations in their bond metrics (Table 2). For example, binding of Na$^+$ or K$^+$ to the phenolate group of **NiL** leads to elongation of both their Ni−O and Ni−N bond distances (i.e., ~0.03 Å for **NiNaL3** and ~0.01 Å for **NiKL4**) compared to those in **NiL2$_{Mes}$**, suggesting that the phenox-yimine ligand donates less electron density to the nickel center when a Lewis acid is bound. In contrast, the nickel primary coordination spheres in **NiL2$_{Mes}$** and **Ni$_2$NaL$_2$**, which are not interacting with an alkali metal ion, have nearly identical metal−ligand bond lengths.
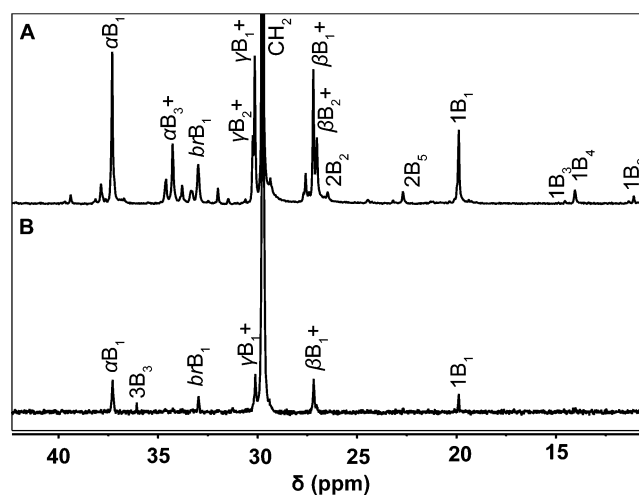
Ethylene Polymerization. The **NiL** complexes were investigated as single-component catalysts in olefin polymerization (Table 3). Upon treatment with the phosphine scavenger Ni(COD)$_2$ (COD = 1,5-cyclooctadiene) in toluene under 100 psi of ethylene, all of the **NiL** complexes produced semicrystalline polyethylene with a turnover frequency (TOF)

Table 2. Comparison of the Bond Distances (Å) and Angles (deg) between the X-ray Structures of the Nickel Complexes

bond lengths (Å) /angles (deg)	$NiL2_{Mes}$	NiNaL3	NiKL4	Ni_2NaL2_2
Ni—O	1.9195(7)	1.952(2)	1.929(2)	1.909(4)
				1.895(4)
Ni—N	1.9310(8)	1.960(3)	1.938(2)	1.920(5)
				1.929(5)
Ni—C	1.912(1)	1.899(3)	1.889(3)	1.898(7)
				1.890(6)
Ni—P	2.1794(3)	2.194(1)	2.1656(9)	2.176(2)
				2.176(2)
N—Ni—C	95.13(4)	91.9(1)	92.8(1)	94.5(2)
				94.2(3)
O—Ni—P	85.65(2)	85.8(1)	86.48(6)	89.9(1)
				89.1(2)

Figure 5. Representative ^{13}C NMR spectra (TCE-d_2, 150 MHz, 120 °C) of (A) amorphous and (B) semicrystalline polyethylene obtained in this work. Peak assignments were made according to ref 49. Branches are given the label xBy, where y is the branch length and x is the carbon number starting from the methyl group as 1. Greek letters and "br" are used instead of x for the methylene carbons in the polymer backbone and a branch point, respectively. The (+) sign indicates overlapping signals.

of ∼2.7 × 10³ g/(mol Ni·h) (entries 1, 5, 9, and 15), which is similar to other nickel phenoxyimine catalysts reported in the literature.[14,21] Characterization by quantitative ^{13}C NMR spectroscopy[48−50] indicates that the polyethylene obtained contains ∼20 branches per 1000 carbon atoms and comprises mostly methyl branches (∼75−100%, Figure 5B). Gel permeation chromatography (GPC) analysis indicates that their molecular weights (M_n) are in the range of (2.32−4.36) × 10³ g/mol with polydispersities (M_w/M_n) between 1.4 and 1.8. These data suggest that the **NiL** complexes are nonliving single-site catalysts. Because **NiL2−NiL4** (entries 5, 9, and 15, respectively) exhibit nearly the same activity as the parent **NiL0** compound (entry 1), it appears that having additional PEG chains in the **NiL** structures neither promote nor inhibit polymerization.

Next, the influence of salt additives on ethylene polymerization by the **NiL** catalysts was examined. The nickel−alkali complexes were preassembled by combining **NiL** and MBAr$^F_4$ (1:1.1) in toluene and then stirred for 30 min to give a clear

yellow-orange solution. The mixture was then treated with Ni(COD)₂ and then charged with ethylene in a high-pressure glass reactor. The polymerization data are shown in Table 3. Addition of Li⁺, Na⁺, or K⁺ salts to **NiL0** or **NiL2** led to a *decrease* (entries 2−4 and 6−8), whereas the addition of Na⁺ or K⁺ to **NiL3** or **NiL4** (entries 11, 12, 17) led to an *increase* in TOF compared to polymerizations performed in the absence of salt additives. The highest activity was achieved using **NiL4** with Na⁺ (TOF = 47 × 10³ g/(mol Ni·h), entry 17), which is a ∼20-fold enhancement compared to polymerizations performed without Na⁺ (entry 15). When reactions were carried

Table 3. Polymerization Data for NiL0, NiL2−NiL4[a]

entry	cat.	salt	polymer yield (mg)	TOF (× 10³ g/(mol·h))	polymer type	branches (/1000 C)[b]	C_1 (%)[c]	C_2 (%)[c]	C_3 (%)[c]	C_4^+ (%)[c]	M_n (× 10³)[d]	M_w/M_n[d]
1	**NiL0**	none	67	2.8	semi-crystalline	26	100	0	0	0	4.36	1.8
2	**NiL0**	Li⁺	10	0.40	semi-crystalline	-	-	-	-	-	-	-
3	**NiL0**	Na⁺	0.5	0.02	semi-crystalline	-	-	-	-	-	-	-
4	**NiL0**	K⁺	53	2.2	semi-crystalline	-	-	-	-	-	3.24	1.5
5	**NiL2**	none	60	2.5	semi-crystalline	16	100	0	0	0	2.32	1.4
6	**NiL2**	Li⁺	5	0.2	semi-crystalline	-	-	-	-	-	-	-
7	**NiL2**	Na⁺	6	0.3	semi-crystalline	-	-	-	-	-	-	-
8	**NiL2**	K⁺	4	0.2	semi-crystalline	-	-	-	-	-	-	-
9	**NiL3**	none	67	2.8	semi-crystalline	20	75	13	2	10	2.65	1.4
10	**NiL3**	Li⁺	32	1.4	semi-crystalline	-	-	-	-	-	-	-
11	**NiL3**	Na⁺	160	6.7	amorphous	107	81	7	1	11	7.69	2.3
12	**NiL3**	K⁺	75	3.1	amorphous	106	73	11	3	13	3.02	2.8
13[e]	**NiL3**	Mg²⁺	50	2.1	semi-crystalline	17	90	0	0	10	-	-
14[e]	**NiL3**	Ca²⁺	59	2.5	semi-crystalline	24	84	0	0	16	-	-
15	**NiL4**	none	67	2.8	semi-crystalline	19	100	0	0	0	3.01	1.5
16	**NiL4**	Li⁺	28	1.2	amorphous	-	-	-	-	-	-	-
17	**NiL4**	Na⁺	1130	47	amorphous	82	79	7	1	13	4.66	2.3
18	**NiL4**	K⁺	5	0.2	semi-crystalline	-	-	-	-	-	-	-

[a]Polymerization conditions: nickel precatalyst (24 μmol), Ni(COD)₂ (48 μmol), MBAr$^F_4$ (26 μmol, if any), ethylene (100 psi), 5 mL toluene, 1 h at RT. [b]The total number of branches per 1000 carbons was determined by ^1H NMR spectroscopy. [c]Branching ratio was determined by ^{13}C NMR spectroscopy. [d]Determined by GPC in trichlorobenzene or decalin at 140 °C. [e]The salt additive is poorly soluble in toluene.

Table 4. Polymerization Time Study for NiL3[a]

entry	cat.	salt	time (h)	polymer yield (mg)	TOF ($\times 10^3$ g/(mol·h))	branches (/1000 C)[b]	C_1 (%)[c]	C_2 (%)[c]	C_3 (%)[c]	C_4^+ (%)[c]	M_n ($\times 10^3$)[d]	M_w/M_n[d]
1	**NiL3**	none	0.5	53	4.4	20	75	13	2	10	2.48	1.2
2	**NiL3**	none	1	67	2.8	25	69	13	4	14	2.65	1.4
3	**NiL3**	none	2	84	1.8	24	66	21	2	11	2.95	1.4
4	**NiL3**	none	3	83	1.2	31	44	26	6	24	2.51	1.4
5	**NiL3**	Na$^+$	0.5	120	10.0	115	79	7	3	11	9.87	2.0
6	**NiL3**	Na$^+$	1	160	6.7	107	81	7	1	11	7.69	2.3
7	**NiL3**	Na$^+$	2	330	6.8	100	80	6	3	11	9.58	2.1
8	**NiL3**	Na$^+$	3	440	6.1	105	82	5	2	11	9.93	2.3

[a]Polymerization conditions: **NiL3** (24 μmol), Ni(COD)$_2$ (48 μmol), NaBAr$^F_4$ (26 μmol, if any), ethylene (100 psi), 5 mL toluene, at RT. [b]The total number of branches per 1000 carbons was determined by ^{1}H NMR spectroscopy. [c]Branching ratio was determined by ^{13}C NMR spectroscopy. [d]Determined by GPC in trichlorobenzene or decalin at 140 °C.

out using **NiL0**, NaBAr$^F_4$, and tetraethylene glycol dimethyl ether (1:1.1:2) instead of **NiL4**/NaBAr$^F_4$, no increase in productivity was observed, indicating that the sodium-PEG group must be attached to **NiL** in order to interact with the catalyst in a synergistic manner. The different effects of M$^+$ on different **NiL** variants seem to correlate well with the stabilities of their bimetallic [NiM(Ph)(PPh$_3$)(L)](BAr$^F_4$) (**NiML**) species and their propensities to form [Ni$_2$M-(Ph)$_2$(PPh$_3$)$_2$(L)$_2$](BAr$^F_4$) (**Ni$_2$ML$_2$**) complexes (vide infra). Polymerizations were also attempted using dicationic salts, such as Mg(SO$_3$CF$_3$)$_2$ and Ca(SO$_3$CF$_3$)$_2$ (entries 13 and 14, respectively); unfortunately, the alkaline salts have poor solubility in toluene and could not form discrete nickel-alkaline complexes in this solvent.

Interestingly, polymerizations by **NiL**/M$^+$ that show an increase in TOF yielded amorphous rather than semicrystalline polyethylene (entries 11, 12, 17). Analysis by NMR spectroscopy reveals that the amorphous polymer is highly branched, with ~80−110 branches per 1000 carbon atoms (Figure 5A).[51] The polymer branches vary in length, with an appreciable amount of C$_4^+$ chains (~10% of all branches). The amorphous polyethylenes have M_n values of (3.02−7.69) × 10^3 g/mol and M_w/M_n between 2.3 and 2.8. The significantly different polymer morphologies afforded by **NiL** with and without M$^+$ clearly indicate that the cationic additives have a direct influence on the coordination−insertion process during catalysis.

To evaluate the stability of the **NiL** catalysts, polymerization studies were conducted in increments of 0.5, 1, 2, and 3 h (Table 4). In the absence of alkali salts, **NiL3** produced semicrystalline polyethylene with an average M_n of ~2.6 × 10^3 g/mol and M_w/M_n of ~1.4. These values remained relatively constant over the course of 3 h (entries 1−4). The gradual decline in TOF during this same time period suggests that **NiL3** decomposes slowly, possibly due to the formation of inactive nickel-bis(phenoxyimine) species.[52] In the presence of Na$^+$, **NiL3** consistently yielded amorphous polyethylene with an M_n of ~9.3 × 10^3 g/mol and M_w/M_n of ~2.2, which suggests that the **NiNaL3** catalyst is nonliving and that M_n is limited by the rate of chain transfer. Analysis by NMR spectroscopy shows that the polymer branching structures are unaffected by the polymerization time (entries 5−8). The reaction of **NiL3**/NaBAr$^F_4$/Ni(COD)$_2$ with ethylene also shows a slight decrease in TOF over a 3 h period, but to a lesser extent than in the absence of added Na$^+$. It is possible that the heterobimetallic nickel−sodium complex is less susceptible to formation of inactive nickel-bis(phenoxyimine) species compared to the

mononickel complex but further studies are needed to clarify. It should be possible to improve the catalyst stability by increasing the steric bulk of the phenoxyimine ligand,[2,11] which we aim to do in future work.

Structure−Activity Correlation. A plot of the TOF of the **NiL** catalysts (Table 3) versus their association constants K_{a1} with various alkali cations (Table 1) suggests that there is a strong correlation between one another (Figure 6). For
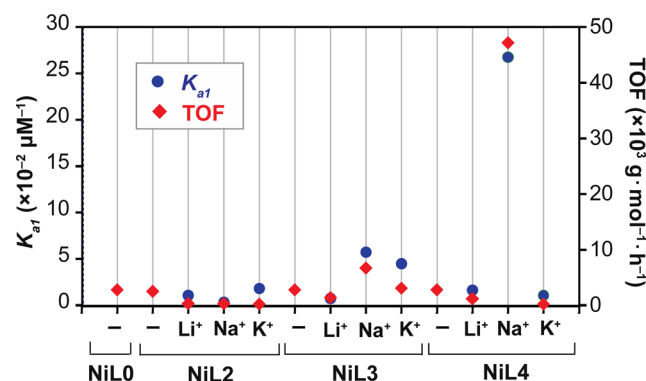
Figure 6. Structure−activity correlation plot showing the effect of different cations (Li$^+$, Na$^+$, and K$^+$) on the ethylene polymerization activity of the **NiL** variants. The association constants K_{a1} are shown as blue dots, whereas the TOFs are shown as red diamonds. Entries on the x-axis denoted with (−) indicate that no salt additives were present.

example, **NiL3** and Li$^+$ has a K_{a1} value of 0.77 × 10^{-2} μM^{-1} and TOF of 1.4 × 10^3 g/(mol Ni·h), whereas **NiL3** and Na$^+$ has a K_{a1} value of 5.74 × 10^{-2} μM^{-1} and TOF of 6.7 × 10^3 g/(mol Ni·h). The ~7-fold increase in stability of **NiNaL3** compared to **NiLiL3** also shows ~5-fold increase in polymerization activity. This trend is most apparent for **NiL4**, which exhibits the strongest binding to sodium (K_{a1} = 26.66 × 10^{-2} μM^{-1}) and gave the highest polymerization activity when Na$^+$ was used as an additive (TOF = 47 × 10^3 g/(mol Ni·h)). In contrast, the lower affinity of **NiL4** for lithium (K_{a1} = 1.65 × 10^{-2} μM^{-1}) and potassium (K_{a1} = 1.83 × 10^{-2} μM^{-1}) compared to for sodium, yielded significantly less active polymerization catalysts (i.e., ~39-fold and ~235-fold decrease in TOF, respectively, compared to Na$^+$). We hypothesize that the dinuclear **NiML** species are responsible for the enhancement in polymerization activity and changes in polymer microstructure (Scheme 2). It should be noted that the **NiL** species can dimerize in the presence of M$^+$ to furnish trinuclear

Ni_2ML_2 complexes (K_{a2}, Table 1), which may also be involved in polymerization.

Scheme 2. Proposed Model for the Reaction of NiL with Ethylene in the Presence and Absence of Alkali Metal Ions
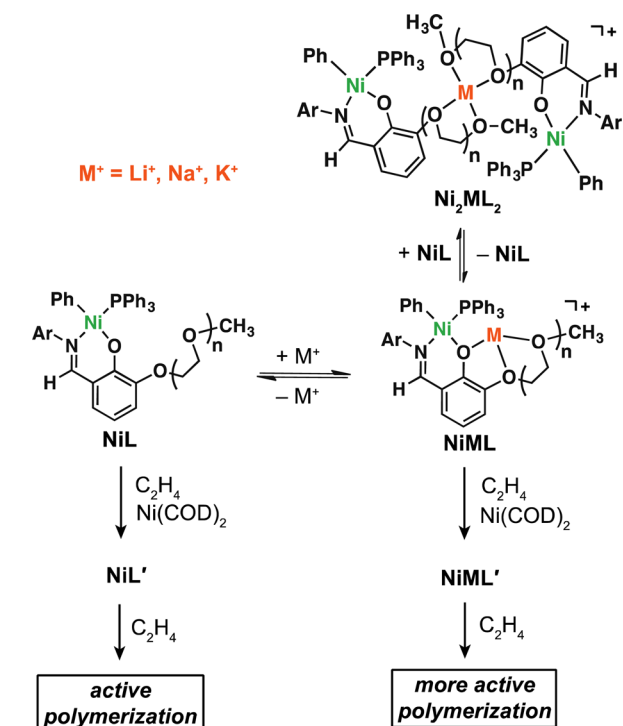
A possible reaction model for the polymerization of ethylene by the **NiL** complexes is depicted in Scheme 2. We have demonstrated that when **NiL** is treated with $Ni(COD)_2$ ethylene polymerization can take place, presumably through the formation of nickel-ethylene intermediates (**NiL′**). When an alkali salt is added to **NiL** prior to catalyst activation, either dinuclear **NiML** (e.g., **NiNaL3** and **NiKL4** in Figure 3) or trinuclear Ni_2ML_2 (e.g., Ni_2NaL2_2 in Figure 4) species are generated. The relative ratio of **NiML**:Ni_2ML_2 is determined by their equilibrium distribution (i.e., K_{a1} and K_{a2}). Abstraction of triphenylphosphine from Ni_2ML_2 under ethylene might afford the corresponding bis(ethylene) adduct $Ni_2M-(Ph)_2(C_2H_4)_2(L)_2$ ($Ni_2ML_2′$). We expect that a species such as $Ni_2ML_2′$ would behave similarly to **NiML′** in ethylene polymerization, except that the former is expected to be less catalytically active due to the increased steric environment around its nickel centers. This model might account for the observation that certain combinations of **NiL**/M⁺ yield catalysts that exhibit a lower TOF in ethylene polymerization compared to the mononuclear nickel catalysts. On the other hand, we have also shown that when the ionic radius of M⁺ is a suitable match for the PEG chain in **NiL**, stable dinuclear **NiML** species are obtained. Activation by $Ni(COD)_2$ would yield **NiML′**, which our studies suggest are highly active ethylene polymerization catalysts. We hypothesize that the alkali metal ion enhances the electrophilicity of the nickel center, which appears to result in more efficient olefin binding and insertion as well as faster rates of chain walking. It is also possible that the increased steric bulk of the alkali–PEG unit of the **NiML** complex, compared to **NiL**, may also play a role in modulating its catalytic behavior. At present, we are uncertain to what

extent electronic versus steric effects have on tuning the nickel catalyst's properties. Future studies will seek to determine the identities of the active **NiL′** and **NiML′** species in solution.

CONCLUSIONS

We have synthesized a new site-differentiated phenoxyimine ligand platform containing polyethylene glycol chains for the preparation of heterobimetallic nickel-alkali metal complexes. We showed through metal titration studies that the addition of alkali salts to mononuclear **NiL** complexes resulted in the formation of 1:1 and 2:1 **NiL**:M⁺ species in solution. Structural characterization of the 1:1 complexes by X-ray crystallography demonstrates that the phenoxyimine ligands in both **NiNaL3** and **NiKL4** are metalated to nickel and the PEG chains encapsulate the alkali cation to form discrete molecular structures. Crystals of the 2:1 complex Ni_2NaL2_2 were also analyzed by X-ray diffraction, which reveals that two **NiL2** units are linked via binding to a single sodium cation. Ethylene polymerization studies show that **NiL**/$Ni(COD)_2$ yield slightly branched semicrystalline polyethylene, whereas **NiL**/$MBAr^F_4$/$Ni(COD)_2$ yield highly branched amorphous polyethylene in some cases. The polymerization efficiency of various **NiL**/M⁺ combinations was high when the association constants K_{a1} for their corresponding **NiML** complexes were large, suggesting that they are the catalytically active species. Remarkably, the **NiML** complexes show significant increases in polymerization activity, molecular weight, and branching frequency compared to the mononuclear **NiL** catalysts. These results provide compelling evidence that alkali cations can have a beneficial effect on coordination–insertion polymerization and provide a new design strategy for developing improved catalysts for the copolymerization of ethylene with functional monomers in future work. Further studies will be conducted to obtain a better understanding of the precise role of alkali ions in coordination–insertion polymerization and to explore the generality of this effect on other catalyst systems.

EXPERIMENTAL SECTION

General. Commercial reagents were used as received. All air- and water-sensitive manipulations were performed using standard Schlenk techniques or under a nitrogen atmosphere using a glovebox. Anhydrous solvents were obtained from an Innovative Technology solvent drying system saturated with Argon. High-purity polymer grade ethylene was obtained from Matheson TriGas without further purification. Compound **1A**,[53] **HL0**,[54] $NaBAr^F_4$,[55] $KBAr^F_4$[56] and $NiBr(Ph)(PPh_3)_2$[57] were prepared according to literature procedures. The syntheses of the **HL**/**NaL** ligands and $LiBAr^F_4$ are given in the Supporting Information.

Physical Methods. NMR spectra were acquired using JEOL spectrometers (ECA-400, 500, and 600) and referenced using residual solvent peaks. ³¹P NMR spectra were referenced to phosphoric acid. IR spectra were measured using a Thermo Nicolet Avatar FT-IR spectrometer. High-resolution mass spectra were obtained from the mass spectral facility at the University of Texas at Austin. Gas chromatography–mass spectrometry was performed using an Agilent 7890 GC/5977A MSD instrument equipped with an HP-5MS capillary column. Solution samples for UV–vis absorption measurements were contained in 1 cm septum sealed quartz cuvettes and recorded using an Agilent Cary 60 spectrophotometer. Elemental analyses were performed by Atlantic Microlab.

Synthesis. *Preparation of NiL0.* Inside the glovebox, **NaL0** (91 mg, 0.27 mmol, 1.0 equiv) and $NiBr(Ph)(PPh_3)_2$ (201 mg, 0.27 mmol, 1.0 equiv) were combined in 15 mL of THF. The mixture was stirred at room temperature for 4 h. The resulting red solution was filtered through a pipet plug and then dried under vacuum to give a dark red

oil. Upon the addition of pentane and after the mixture stirred for ~5 min, a yellow solid formed. The solid was isolated by filtration and then washed with fresh pentane. The product was dried to yield a yellow solid (181 mg, 0.26 mmol, 94%). ^{1}H NMR (CDCl$_3$, 400 MHz): δ (ppm) = 7.97 (d, J_{HP} = 8.8 Hz, 1H), 7.53 (t, J_{HH} = 8.4 Hz, 6H), 7.36 (t, J_{HH} = 7.2 Hz, 3H), 7.24 (m, 6H), 6.95 (t, J_{HH} = 7.6 Hz, 1H), 6.86−6.75 (m, 4H), 6.68 (d, J_{HH} = 7.2 Hz, 2H), 6.44 (t, J_{HH} = 7.6 Hz, 1H), 6.23 (t, J_{HH} = 7.6 Hz, 1H), 6.11 (t, J_{HH} = 7.6 Hz, 2H), 3.85 (m, 2H), 3.12 (s, 3H), 1.19 (d, J_{HH} = 6.8 Hz, 6H), 1.10 (d, J_{HH} = 6.4 Hz, 6H). ^{13}C NMR (CDCl$_3$, 100 MHz): δ (ppm) = 165.67, 158.22, 152.80, 149.86, 146.09 (d, J_{CP} = 49 Hz), 140.65, 137.56, 134.50 (d, J_{CP} = 9.7 Hz), 131.59 (d, J_{CP} = 44 Hz), 129.47, 127.79 (d, J_{CP} = 9.7 Hz), 126.35, 125.67, 124.84, 122.52, 120.95, 119.53, 117.03, 112.83, 56.82, 28.65, 25.86, 22.63. ^{31}P NMR (CDCl$_3$, 162 MHz): δ (ppm) = 23.06. UV−vis (Toluene): λ_{max}/nm (ε/cm^{-1} M^{-1}) = 359 (3743). FT-IR: 2961(ν_{CNH}), 1604 (ν_{CN}), 1463, 1446, 1240, 1226, 1172, 746, 731, 692, 531 cm^{-1}. Mp (decomp.) = ~140 °C. Anal. Calcd for C$_{44}$H$_{44}$NNiO$_2$P·(C$_4$H$_8$O)$_{0.15}$(CH$_2$Cl$_2$)$_{0.2}$: C, 73.32; H, 6.32; N, 1.90. Found: C, 73.29; H, 6.37; N, 1.76. *Trace amounts of diethyl ether and dichloromethane, which were used in recrystallization of the material and confirmed by ^{1}H NMR spectroscopy, could not be removed completely by vacuum drying overnight.*

Preparation of NiL2. The same procedure was used as described for **NiL0**, except that **NaL2** (71 mg, 0.17 mmol, 1 equiv) was used instead of **NaL0**. The ligand was combined with 1 equiv of NiBr(Ph)(PPh$_3$)$_2$ (125 mg, 0.17 mmol). The product was isolated as a yellow solid (105 mg, 0.13 mmol, 77%). ^{1}H NMR (CDCl$_3$, 400 MHz): δ (ppm) = 7.96 (d, J_{HP} = 9.2 Hz, 1H), 7.56 (t, J = 8.8 Hz, 6H), 7.33 (t, J_{HH} = 8.4 Hz, 3H), 7.23 (m, 6H), 6.94 (t, J_{HH} = 7.6 Hz, 1H), 6.88−6.83 (m, 4H), 6.55 (d, J_{HH} = 7.2 Hz, 2H), 6.42 (t, J_{HH} = 7.2 Hz, 1H), 6.21 (t, J_{HH} = 7.2 Hz, 1H), 6.07 (t, J_{HH} = 7.2 Hz, 2H), 3.86 (m, 2H), 3.32−3.27 (m, 9H), 2.92 (t, J_{HH} = 5.2 Hz, 2H), 1.12 (d, J_{HH} = 7.2 Hz, 6H), 1.09 (d, J_{HH} = 6.8 Hz, 6H). ^{13}C NMR (CDCl$_3$, 100 MHz): δ (ppm) = 165.47, 158.57, 151.26, 149.66, 145.79 (d, J_{CP} = 50 Hz), 140.64, 136.89, 134.38 (d, J_{CP} = 9.7 Hz), 132.03, 131.60, 129.60, 127.79 (d, J_{CP}= 9.7 Hz), 127.48, 125.72, 124.82, 122.56, 120.86, 119.97, 112.89, 71.92, 70.24, 69.86, 69.22, 59.09, 28.66, 25.78, 22.64. ^{31}P NMR (CDCl$_3$, 162 MHz): δ (ppm) = 22.22. UV−vis (Et$_2$O): λ_{max}/nm (ε/cm^{-1} M^{-1}) = 340 (4870), 416 (3250). FT-IR: 2958 (ν_{CNH}), 1603 (ν_{CN}), 1445, 1436, 1222, 1108, 1093, 744, 729, 529 cm^{-1}. Mp (decomp.) = ~135 °C. Anal. Calcd for C$_{48}$H$_{52}$NNiO$_4$P·(C$_4$H$_8$O): C, 71.90; H, 6.96; N, 1.61. Found: C, 71.82; H, 6.56; N, 1.80. *Trace amounts of diethyl ether, which was confirmed by ^{1}H NMR spectroscopy, could not be removed completely by vacuum drying overnight.*

Preparation of NiL3. The same procedure was used as described for **NiL0**, except that **NaL3** (123 mg, 0.27 mmol, 1 equiv) was used instead of **NaL0**. The ligand was combined with 1 equiv of NiBr(Ph)(PPh$_3$)$_2$ (196 mg, 0.27 mmol). The product was isolated as a yellow solid (208 mg, 0.25 mmol, 93%). ^{1}H NMR (CDCl$_3$, 600 MHz): δ (ppm) = 8.01 (d, J_{HP} = 9.0 Hz, 1H), 7.61 (t, J_{HH} = 9.0 Hz, 6H), 7.35 (t, J_{HH} = 6.6 Hz, 3H), 7.25 (t, J_{HH} = 7.2 Hz, 6H), 6.98 (t, J_{HH} = 7.8 Hz, 1H), 6.93 (t, J_{HH} = 7.2 Hz, 1H), 6.89 (m, 3H), 6.62 (d, J_{HH} = 7.8 Hz, 2H), 6.46 (t, J_{HH} = 7.8 Hz, 1H), 6.25 (t, J_{HH} = 6.6 Hz, 1H), 6.10 (t, J_{HH} = 7.2 Hz, 2H), 3.90 (m, 2H), 3.63 (m, 2H), 3.57 (m, 2H), 3.50 (t, J_{HH} = 4.2 Hz, 2H), 3.42 (s, 3H), 3.35 (m, 4H), 2.97 (t, J_{HH} = 6.0 Hz, 2H), 1.17 (d, J_{HH} = 7.2 Hz, 6H), 1.14 (d, J_{HH} = 6.6 Hz, 6H). ^{13}C NMR (CDCl$_3$, 150 MHz): δ (ppm) = 165.53, 158.68, 151.32, 149.72, 145.81 (d, J_{CP} = 48 Hz), 140.68, 136.94, 134.43 (d, J_{CP} = 10.35 Hz), 131.86 (d, J_{CP} = 44 Hz), 129.67, 128.49, 127.86 (d, J_{CP} = 8.85 Hz), 127.61, 125.80, 124.90, 122.62, 121.06 (d, J_{CP} = 32 Hz), 120.07, 112.98, 72.09, 70.66, 70.62, 70.40, 69.92, 69.27, 59.21, 28.72, 25.84, 22.71. ^{31}P NMR (CDCl$_3$, 243 MHz): δ (ppm) = 22.23. UV−vis (Et$_2$O): λ_{max}/nm (ε/cm^{-1} M^{-1}) = 340 (4400), 416 (2950). FT-IR: 2957(ν_{CHN}), 1602 (ν_{CN}), 1462, 1435, 1243, 1223, 1095, 742, 729, 692, 531 cm^{-1}. Mp (decomp.) = ~102 °C. Anal. Calcd for C$_{50}$H$_{56}$NNiO$_5$P: C, 71.44; H, 6.71; N, 1.67. Found: C, 71.16; H, 6.63; N, 1.62.

Preparation of NiL4. Inside the glovebox, **NaL4** (68 mg, 0.13 mmol, 1.0 equiv) and NiBr(Ph)(PPh$_3$)$_2$ (99 mg, 0.13 mmol, 1.0 equiv) were combined in 10 mL of THF. The mixture was stirred at room temperature for 4 h. The resulting red solution was filtered

through a pipet plug and then dried under vacuum to give a dark red oil. The product was washed with a small amount of pentane to remove triphenylphosphine; however, **NiL4** is also somewhat soluble in pentane and trace amounts of triphenylphosphine (<5%) could not be removed completely. The product was isolated as a red viscous material and used without further purification (89 mg, 0.10 mmol, ~75%). ^{1}H NMR (CDCl$_3$, 400 MHz): δ (ppm) = 7.96 (d, J_{HP} = 8.8 Hz, 1H), 7.55 (t, J_{HH} = 9.2 Hz, 6H), 7.33(m, 3H), 7.21 (m, 6H), 6.94 (t, J_{HH} = 8.4 Hz, 1H), 6.88−6.83 (m, 4H), 6.57 (d, J_{HH} = 7.6 Hz, 2H), 6.42 (t, J_{HH} = 7.6 Hz, 1H), 6.20 (t, J_{HH} = 6.8 Hz, 1H), 6.05 (t, J_{HH} = 7.6 Hz, 2H), 3.85 (m, 2H), 3.67−3.60 (m, 6H), 3.55 (m, 2H), 3.44 (t, J_{HH} = 4.5 Hz, 2H), 3.38 (s, 3H), 3.29 (m, 4H), 2.91 (t, J_{HH} = 5.6 Hz, 2H), 1.12 (d, J_{HH} = 7.2 Hz, 6H), 1.09 (d, J_{HH} = 6.8 Hz, 6H). ^{13}C NMR (CDCl$_3$, 100 MHz): δ (ppm) = 165.47, 158.62, 151.25, 149.66, 145.78 (d, J_{CP} = 49 Hz), 140.64, 136.87, 134.47 (d, J_{CP} = 9.7 Hz), 132.01, 131.58, 129.61, 128.82, 127.76 (d, J_{CP} = 9.8 Hz), 125.73, 124.83, 122.56, 120.98 (d, J_{CP} = 21 Hz), 120.01, 112.89, 72.04, 70.69, 70.64, 70.61, 70.56, 70.34, 69.84, 69.22, 59.18, 28.67, 25.78, 22.64. ^{31}P NMR (CDCl$_3$, 162 MHz): δ (ppm) = 22.21. UV−vis (Et$_2$O): λ_{max}/nm (ε/cm^{-1} M^{-1}) = 340 (4500), 416 (2930). FT-IR: 2857(ν_{CHN}), 1603(ν_{CN}), 1461, 1434, 1244, 1223, 1093, 741, 692, 530 cm^{-1}.

Metal Titration Studies. Stock solutions of **NiL** and MBAr$^F_4$ salts (M = Li$^+$, Na$^+$, K$^+$) were prepared inside of the glovebox. The 500 μM stock solutions of **NiL** were obtained by dissolving 25 μmol of **NiL** in 50 mL of Et$_2$O. A 10 mL aliquot of this 500 μM solution was diluted to 50 mL using a volumetric flask to give a final concentration of 100 μM. The 3.0 mM stock solutions of MBAr$^F_4$ were obtained by dissolving 30 μmol of MBAr$^F_4$ in 10 mL of Et$_2$O using a volumetric flask. A 3.0 mL solution of **NiL** was transferred to a 1 cm quartz cuvette and then sealed with a septum screw cap. A 100 μL airtight syringe was loaded with the 3.0 mM solution of MBAr$^F_4$. The cuvette was placed inside a UV−vis spectrophotometer and the spectrum of the **NiL** solution was recorded. Aliquots containing 0.1 equiv of MBAr$^F_4$ (10 μL), relative to **NiL**, were added and the solution was allowed to reach equilibrium before the spectra were measured (~20−30 min). The titration studies were stopped after the addition of up to 4.0 equiv of MBAr$^F_4$. The spectral data were corrected for dilution and the binding model and binding constants were determined using the program DynaFit.[41] The data analysis procedure using DynaFit is provided in the Supporting Information.

Ethylene Polymerization. Inside the glovebox, solid **NiL** (24 μmol) and MBAr$^F_4$ (26 μmol) were dissolved in 5 mL of toluene and stirred for 30 min. Solid Ni(COD)$_2$ (48 μmol) was added and the solution was transferred to a Fischer−Porter glass vessel along with a magnetic stir bar and then the reactor was sealed. The high-pressure apparatus was removed from the glovebox and then securely fastened on top of a stir plate. The ethylene line was attached and the reactor was purged with ethylene three times by pressurizing with ethylene and then releasing the pressure. The reactor was then pressurized to 100 psi of ethylene and stirred at room temperature (RT) for a specified amount of time. The ethylene line was closed and the vessel was slowly vented. About 1 mL of HCl(aq) was added, followed by the addition of 2 mL of MeOH. The aqueous layer was removed by pipetting and the organic layer was evaporated to dryness under vacuum. The resulting material was washed with MeOH and CH$_2$Cl$_2$ and then dried under vacuum.

Polymer Characterization. Analysis of Molecular Weight (M_n) and Total Branching by ^{1}H NMR Spectroscopy. The NMR samples contained ~10−20 wt % of polymer in 1,1,2,2-tetrachlorethane-d_2 and were recorded at 600 MHz using standard acquisition parameters (120 °C). The M_n values were determined using the method described by Daugulis and Brookhart,[58] and the total number of branches per 1000 carbons ($N_{branches}$) were determined by the method described by Mecking and co-workers.[59]

Analysis of Branching Ratio by Quantitative ^{13}C NMR Spectroscopy. The NMR samples contained ~10−20 wt % of polymer and 50 mM chromium acetylacetonate Cr(acac)$_3$ in 1,1,2,2-tetrachlorethane-d_2 and were recorded at 150 MHz (120 °C). For solid polymers, the samples were acquired using a 70° pulse of 9.25 μs, a relaxation delay of 0 s, an acquisition time of 0.67 s, and inverse gated decoupling. The

T_1 values of the carbon atoms were measured to be 0.7 s. For amorphous polymers, the samples were acquired using an 80° pulse of 10.58 µs, a relaxation delay of 0 s, an acquisition time of 0.67 s, and inverse gated decoupling. The T_1 values of the carbon atoms were measured to be 0.4 s. The samples were preheated for 15 min prior to data acquisition. The carbon spectra were assigned based on the chemical shift values reported in the literature.[49] The branch ratios were determined by dividing the integrated value for a type of branch end over the total number of branches.

Analysis of Molecular Weight (M_n, M_w) and Polydispersity (M_n/M_w) by Gel Permeation Chromatography (GPC). GPC analyses were performed using a Malvern high temperature GPC instrument equipped with refractive index, viscometer, and light scattering detectors. Polyethylene samples were prepared with a concentration of ~30 mg of polymer in 10 mL of solvent. The solid polymers were predissolved in decalin at 135 °C for at least 1 h before injection, whereas the amorphous polymers were predissolved in 1,2,4-trichlorobenzene (TCB) at 135 °C for at least 1 h before injection. Samples were acquired at 140 °C using TCB as the mobile phase. A calibration curve was established with polystyrene standards. All the samples measured yielded refractive index increments (dn/dc) of 0.08−0.10, which are consistent with the reported value of 0.1 for polyethylene.[60]

X-ray Crystallography. Single crystals of **NiL2$_{Mes}$** were grown from vapor diffusion of pentane into a solution of the complex in benzene, whereas single crystals of **NiNaL3**, **NiKL4**, and **Ni$_2$NaL2$_2$** were grown from saturated solutions of the complexes in Et$_2$O/pentane. The crystals were mounted at 123 K on a Bruker diffractometer equipped with a CCD APEX II detector using Mo Kα radiation. Data reduction was performed within the APEX II software and empirical absorption corrections were applied using SADABS. The structures were solved by Direct methods in SHELXS and refined by full-matrix least-squares based on F^2 using SHELXL. All non-hydrogen atoms were located and refined anisotropically. Hydrogen atoms were fixed using a riding model and refined isotropically. Additional crystallographic details are provided in the Supporting Information, including a summary of the crystallographic data in Table S1.

■ ASSOCIATED CONTENT

ⓢ Supporting Information

The Supporting Information is available free of charge on the ACS Publications website at DOI: 10.1021/jacs.5b10351.

> Synthesis procedures and characterization, metal titration data and fitting plots (CIF)
> X-ray crystallographic summary (PDF)

■ AUTHOR INFORMATION

Corresponding Author
*loido@uh.edu

Notes
The authors declare no competing financial interest.

■ ACKNOWLEDGMENTS

■ REFERENCES

(1) Ittel, S. D.; Johnson, L. K.; Brookhart, M. *Chem. Rev.* **2000**, *100*, 1169.

(2) Carrow, B. P.; Nozaki, K. *Macromolecules* **2014**, *47*, 2541.

(3) Nakamura, A.; Anselment, T. M. J.; Claverie, J.; Goodall, B.; Jordan, R. F.; Mecking, S.; Rieger, B.; Sen, A.; van Leeuwen, P. W. N. M.; Nozaki, K. *Acc. Chem. Res.* **2013**, *46*, 1438.

(4) Nakamura, A.; Ito, S.; Nozaki, K. *Chem. Rev.* **2009**, *109*, 5215.

(5) Piers, W. E.; Collins, S. *Comp. Organomet. Chem. III* **2007**, *1*, 141.

(6) Coates, G. W. *J. Chem. Soc., Dalton Trans.* **2002**, 467.

(7) Boffa, L. S.; Novak, B. M. *Chem. Rev.* **2000**, *100*, 1479.

(8) Chen, E. Y.-X. *Chem. Rev.* **2009**, *109*, 5157.

(9) Hustad, P. D. *Science* **2009**, *325*, 704.

(10) Franssen, N. M. G.; Reek, J. N. H.; de Bruin, B. *Chem. Soc. Rev.* **2013**, *42*, 5809.

(11) Gao, R.; Sun, W.-H.; Redshaw, C. *Catal. Sci. Technol.* **2013**, *3*, 1172.

(12) McInnis, J. P.; Delferro, M.; Marks, T. J. *Acc. Chem. Res.* **2014**, *47*, 2545.

(13) Johnson, L. K.; Mecking, S.; Brookhart, M. *J. Am. Chem. Soc.* **1996**, *118*, 267.

(14) Younkin, T. R.; Connor, E. F.; Henderson, J. I.; Friedrich, S. K.; Grubbs, R. H.; Bansleben, D. A. *Science* **2000**, *287*, 460.

(15) Drent, E.; van Dijk, R.; van Ginkel, R.; van Oort, B.; Pugh, R. I. *Chem. Commun.* **2002**, 744.

(16) Camacho, D. H.; Salo, E. V.; Ziller, J. W.; Guan, Z. *Angew. Chem., Int. Ed.* **2004**, *43*, 1821.

(17) Zhang, D.; Nadres, E. T.; Brookhart, M.; Daugulis, O. *Organometallics* **2013**, *32*, 5136.

(18) Rhinehart, J. L.; Mitchell, N. E.; Long, B. K. *ACS Catal.* **2014**, *4*, 2501.

(19) Allen, K. E.; Campos, J.; Daugulis, O.; Brookhart, M. *ACS Catal.* **2015**, *5*, 456.

(20) Chen, Z.; Mesgar, M.; White, P. S.; Daugulis, O.; Brookhart, M. *ACS Catal.* **2015**, *5*, 631.

(21) Zuideveld, M. A.; Wehrmann, P.; Röhr, C.; Mecking, S. *Angew. Chem., Int. Ed.* **2004**, *43*, 869.

(22) Weberski, M. P., Jr.; Chen, C.; Delferro, M.; Zuccaccia, C.; Macchioni, A.; Marks, T. J. *Organometallics* **2012**, *31*, 3773.

(23) Wang, J.; Yao, E.; Chen, Z.; Ma, Y. *Macromolecules* **2015**, *48*, 5504.

(24) Stephenson, C. J.; McInnis, J. P.; Chen, C.; Weberski, M. P., Jr.; Motta, A.; Delferro, M.; Marks, T. J. *ACS Catal.* **2014**, *4*, 999.

(25) Radlauer, M. R.; Agapie, T. *Organometallics* **2014**, *33*, 3247.

(26) Radlauer, M. R.; Buckley, A. K.; Henling, L. M.; Agapie, T. *J. Am. Chem. Soc.* **2013**, *135*, 3784.

(27) Takano, S.; Takeuchi, D.; Osakada, K.; Akamatsu, N.; Shishido, A. *Angew. Chem., Int. Ed.* **2014**, *53*, 9246.

(28) Takeuchi, D.; Chiba, Y.; Takano, S.; Osakada, K. *Angew. Chem., Int. Ed.* **2013**, *52*, 12536.

(29) Takeuchi, D.; Takano, S.; Takeuchi, Y.; Osakada, K. *Organometallics* **2014**, *33*, 5316.

(30) Diamanti, S. J.; Ghosh, P.; Shimizu, F.; Bazan, G. C. *Macromolecules* **2003**, *36*, 9731.

(31) Belle, C.; Pierre, J.-L. *Eur. J. Inorg. Chem.* **2003**, 4137.

(32) Liu, S.; Motta, A.; Mouat, A. R.; Delferro, M.; Marks, T. J. *J. Am. Chem. Soc.* **2014**, *136*, 10460.

(33) Kita, M. R.; Miller, A. J. M. *J. Am. Chem. Soc.* **2014**, *136*, 14519.

(34) Hazari, A.; Labinger, J. A.; Bercaw, J. E. *Angew. Chem., Int. Ed.* **2012**, *51*, 8268.

(35) Cammarota, R. C.; Lu, C. C. *J. Am. Chem. Soc.* **2015**, *137*, 12486.

(36) Kocian, O.; Chiu, K. W.; Demeure, R.; Gallez, B.; Jones, C. J.; Thornback, J. R. *J. Chem. Soc., Perkin Trans. 1* **1994**, 527.

(37) Tsuda, A.; Fukumoto, C.; Oshima, T. *J. Am. Chem. Soc.* **2003**, *125*, 5811.

(38) Tsuda, A.; Oshima, T. *J. Org. Chem.* **2002**, *67*, 1282.

(39) Johnson, L.; Wang, L.; McLain, S.; Bennett, A.; Dobbs, K.; Hauptman, E.; Ionkin, A.; Ittel, S.; Kunitsky, K.; Marshall, W.; McCord, E.; Radzewich, C.; Rinehart, A.; Sweetman, K. J.; Wang, Y.; Yin, Z.; Brookhart, M. In *Beyond Metallocenes*; American Chemical Society: Washington, DC, 2003; Vol. *857*, p 131.

(40) van Truong, N.; Norris, A. R.; Shin, H. S.; Buncel, E.; Bannard, R. A. B.; Purdon, J. G. *Inorg. Chim. Acta* **1991**, *184*, 59.

(41) Kuzmic, P. *Anal. Biochem.* **1996**, *237*, 260.

(42) Lepore, S. D.; Bhunia, A. K.; Cohn, P. *J. Org. Chem.* **2005**, *70*, 8117.

(43) Lu, T.; Yoo, H. K.; Zhang, H.; Bott, S.; Atwood, J. L.; Echegoyen, L.; Gokel, G. W. *J. Org. Chem.* **1990**, *55*, 2269.

(44) Avent, A. G.; Bonafoux, D.; Eaborn, C.; Hill, M. S.; Hitchcock, P. B.; Smith, J. D. *J. Chem. Soc., Dalton Trans.* **2000**, 2183.

(45) Mandai, T.; Tsuzuki, S.; Ueno, K.; Dokko, K.; Watanabe, M. *Phys. Chem. Chem. Phys.* **2015**, *17*, 2838.

(46) Hsu, Y.-L.; Liang, L.-C. *Organometallics* **2010**, *29*, 6201.

(47) Bock, H.; Näther, C.; Havlas, Z.; John, A.; Arad, C. *Angew. Chem., Int. Ed. Engl.* **1994**, *33*, 875.

(48) Bovey, F. A.; Schilling, F. C.; McCrackin, F. L.; Wagner, H. L. *Macromolecules* **1976**, *9*, 76.

(49) Galland, G. B.; de Souza, R. F.; Mauler, R. S.; Nunes, F. F. *Macromolecules* **1999**, *32*, 1620.

(50) Hansen, E. W.; Blom, R.; Bade, O. M. *Polymer* **1997**, *38*, 4295.

(51) Dong, Z.; Ye, Z. *Polym. Chem.* **2012**, *3*, 286.

(52) Connor, E. F.; Younkin, T. R.; Henderson, J. I.; Waltman, A. W.; Grubbs, R. H. *Chem. Commun.* **2003**, 2272.

(53) Kessar, S. V.; Gupta, Y. P.; Mohammad, T.; Goyal, M.; Sawal, K. K. *J. Chem. Soc., Chem. Commun.* **1983**, 400.

(54) Upadhyay, A.; Vaidya, S.; Venkatasai, V. S.; Jayapal, P.; Srivastava, A. K.; Shanmugam, M.; Shanmugam, M. *Polyhedron* **2013**, *66*, 87.

(55) Brookhart, M.; Grant, B.; Volpe, A. F., Jr. *Organometallics* **1992**, *11*, 3920.

(56) Buschmann, W. E.; Miller, J. S.; Bowman-James, K.; Miller, C. N. *Inorg. Synth.* **2002**, *33*, 83.

(57) Standley, E. A.; Smith, S. J.; Müller, P.; Jamison, T. F. *Organometallics* **2014**, *33*, 2012.

(58) Daugulis, O.; Brookhart, M.; White, P. S. *Organometallics* **2002**, *21*, 5935.

(59) Wiedemann, T.; Voit, G.; Tchernook, A.; Roesle, P.; Göttker-Schnetmann, I.; Mecking, S. *J. Am. Chem. Soc.* **2014**, *136*, 2078.

(60) American Polymer Standards Corporation. Light Scattering dn/dc Values. http://www.ampolymer.com/dn-dcValues.html (accessed September 28, 2015).